Research in Pharmaceutical Sciences, June 2025; 20(3): 392-407
Received: 29-01-2025
Peer Reviewed: 25-02-2025
Revised: 13-04-2025
Accepted: 04-05-2025
Published: 17-06-2025

School of Pharmacy & Pharmaceutical Sciences
Isfahan University of Medical Sciences

Original Article

Repurposing FDA-approved drugs to find a novel inhibitor of alpha-ketoglutarate-dependent dioxygenase FTO to treat esophageal cancer

Zeinab Mohammadi[1,2], Marie Saghaeian Jazi[1,3], Seyyed Mehdi Jafari[1,2], Seyyed Mostafa Mir[1,2], Jahanbakhsh Asadi[1,2,*], and Massoud Amanlou[4,*]

[1]*Metabolic Disorders Research Center, Biomedical Research Institute, Golestan University of Medical Sciences, Gorgan, Iran.*
[2]*Department of Clinical Biochemistry, School of Medicine, Golestan University of Medical Sciences, Gorgan, Iran.*
[3]*Stem Cell Research Center, Golestan University of Medical Sciences, Gorgan, Iran.*
[4]*Department of Medicinal Chemistry, Faculty of Pharmacy, Tehran University of Medical Sciences, Tehran, Iran.*

Abstract

Background and purpose: The Fat mass and obesity-associated protein (FTO) plays a significant role in esophageal cancer by regulating N6-methyladenosine (m6A) modification. FTO inhibition has shown potential in cancer therapies but remains underexplored. This study aimed to identify a safer, FDA-approved compound for FTO inhibition that can be used in combination with chemotherapy drugs.
Experimental approach: FDA-approved drugs were screened from the Zinc15 database using AutoDock Vina against the 3D structure of FTO (PDB ID: 3LFM). Discovery Studio software was used to determine binding interactions. The GROMACS package was used for molecular dynamics simulations. A non-toxic concentration was determined through an MTT assay on KYSE-30 esophageal cancer cells. The ELISA assay was used to measure the m6A levels in RNA.
Findings/Results: Four compounds, ergotamine, midazolam, digoxin, and loratadine, were identified. Loratadine (ΔG: -8.9) formed stable interactions with FTO, specifically with residues Ser229, Tyr109, Leu109, Val229, and His231. Molecular dynamic simulations of the FTO-loratadine complex revealed higher RMSD fluctuations (0.4-0.6 nm), but the system remained stable overall. RMSF analysis showed similar fluctuation patterns in all three systems, indicating that loratadine did not affect protein structure stability. MM/PBSA calculations revealed powerful binding energy for the FTO-loratadine complex (-135.73 kJ/mol), driven by favorable van der Waals interactions. KYSE-30 cells treated with loratadine (100 µM), m6A levels in KYSE-30 cells compared to the control group were significantly elevated at a non-toxic concentration.
Conclusion and implications: Loratadine is a promising, low-toxic FTO inhibitor that could complement chemotherapy for esophageal cancer.

Keywords: AutoDock Vina; Drug repurposing; Esophageal cancer; Fat mass and obesity associated protein; Molecular dynamics simulation; N6-methyl adenosine.

INTRODUCTION

RNA modifications play a vital role in various cellular functions, such as cell proliferation, survival, and differentiation. N6-methyladenosine (m6A) is one of the most abundant modifications of messenger RNA (mRNA) in both eukaryotes and humans. It influences RNA splicing, intracellular transport, translation, and cytoplasmic degradation (1, 2).

m6A is a dynamic and reversible modification, and changes in its presence on mRNA determine the RNA's fate, ultimately influencing RNA expression and protein synthesis, or leading to RNA degradation and reduced protein production. Therefore, identifying the proteins involved in this process is crucial, and inhibiting these proteins could be a valuable strategy in the treatment of various diseases and malignancies, including several types of cancers such as esophageal, hepatocellular, and breast cancer.

*Corresponding authors:
J. Asadi, Tel: +98-173243031, Fax: +98-1732430319
Email: dr.asadi@goums.ac.ir
M. Amanlou, Tel: +98-2166959067, Fax: +98-2164121111
Email: amanlou@tums.ac.ir

Access this article online

Website: http://rps.mui.ac.ir

DOI: 10.4103/RPS.RPS_9_25

Methyltransferase and demethylase enzymes regulate m6A levels in RNA, enabling reversible and dynamic modification. Methyltransferases such as N6-methyl adenosine methyltransferase 16 (METTL16) and the complex METTL3/METTL14/Wilm's tumor 1-associating protein (WTAP) are m6A writer proteins (3-5). RNA m6A eraser enzymes, such as fat and obesity-associated protein (FTO) (6, 7) and alkylation repair homolog protein 5 (ALKBH5) (8), remove m6A modifications from RNA molecules. Additionally, m6A readers play a critical role in determining the fate of RNA after translation. The YTHD family (YTHDF 1-3) and two members of the YTHDC family (YTHDC 1-2) are classified as readers (Fig. 1) (9).

Several studies revealed that FTO was the first reported m6A demethylase protein related to body mass and obesity in humans (10, 11). Jia *et al*. demonstrated that FTO is primarily located in nuclear speckles and that m6A in nuclear RNA is the physiological substrate for FTO (6). Multiple functions affected by FTO, such as glycolysis (12), and adipogenesis (13), through the removal of the methyl group from N6-adenosine in RNA. Likewise, elevated FTO activity leads to decreased m6A levels in RNA and impairs cell cycle progression, disrupting normal lineage commitment and functional stem cell differentiation. This results in neurogenesis retardation, immune deficiency, infertility, and cancer progression and migration (14-16). Recent studies have shown that FTO levels are elevated in esophageal cancer cells, which is associated with poor prognosis in esophageal cancer patients (17), tumorigenesis (18), and migration (19). Currently, numerous studies have investigated FTO inhibitors, both specific and nonspecific properties, such as rhein, meclofenamic acid, MO-I-500, fluorescein, and R-2HG (16, 20-25).

Drug repurposing, also known as drug repositioning, is a strategy in drug development that involves identifying new uses for existing drugs beyond their original indications (26). This approach can significantly accelerate the discovery process and reduce costs compared to developing entirely new drugs. Numerous medications have been recently investigated and approved for new therapeutic uses, often utilizing their established safety profiles and pharmacokinetics. In recent years, drug repurposing has gained popularity as a practical approach to address unresolved medical needs effectively (27). Given the significant association between FTO and pathological conditions, we focused on identifying a potential inhibitor of FTO demethylase. This research aimed to discover a novel FTO inhibitor from FDA-approved drugs. Additionally, we evaluated the FTO inhibitory effect of the candidate compound on the KYSE-30 cell line using the MTT assay and measured the m6A content in total RNA isolated from the treated cells.

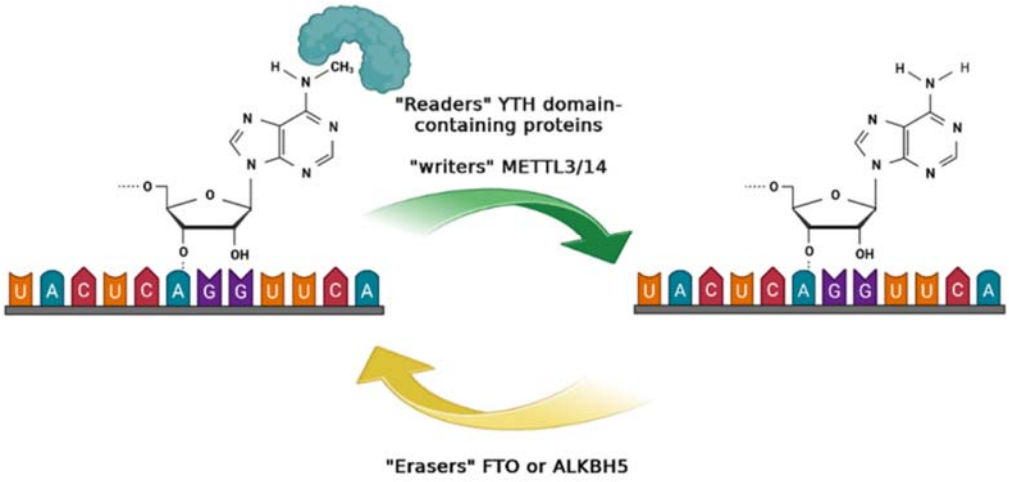

Fig. 1. A schematic diagram illustrates the roles of m6A writers, readers, and erasers in the post-transcriptional regulation of mRNA.

MATERIALS AND METHODS

Virtual screening

The FTO crystal structure was obtained from the RCSB database with PDB ID: 3LFM. The receptor input file was prepared using the AutoDock Tools (ADT) 1.5.6 package (28). The crystal structure of the receptor file was prepared by excluding water molecules and ligands. Hydrogens were then included, and the molecules were modeled in three dimensions. Nonpolar hydrogens were merged, and Kollman charges were assigned and saved in the pdbqt format (29). The binding free energies and the conformation of the ligand within the specified active site were determined using AutoDock Vina 1.2.3 (30). The initial phase involved blind docking to explore the potential binding mode of 3-methylthymidine (3DT) on 3LFM using the entire 3D protein. Furthermore, the 3D structures of FDA-approved small molecules were downloaded from the open-source chemistry Zin15 database (http://zinc15.docking.org) and prepared in pdbqt format using the OpenBabel module (31). The grid box dimensions were assigned 45 × 45 × 45 Å (x, y, and z) with a grid center of 29.773, 7.641, and -28.097 (x, y, and z). Virtual screening was performed using AutoDock Vina 1.2.3 version.

Molecular dynamics simulation

The interaction between FTO and the candidate compound was performed in a dynamic environment determined by molecular dynamics (MD) simulation using the GROMACS 2021.4 package (32). Free FTO and FTO complexed with 3DT (as the main ligand in the protein binding pocket of crystallography structure) and with candidate compound in a water-filled triclinic box were simulated using the Amber99SB force field (33). Moreover, the systems were placed in a solubility transferable intermolecular potential with a 3-point water molecule (tip3p). To adjust the charge neutrality, Na^+ and Cl^- ions were added to each system. Energy minimization was applied to each system with the steepest descent algorithm. Temperature and pressure were maintained using the Nose-Hoover thermostat and a Berendsen barostat, respectively. Besides, the equilibrium of NVT and NPT was performed (34-38). The interactions, electrostatics, and covalent bond constraints were calculated using the Lennard-Jones potential, the Particle-mesh Ewald (PME) method, and the Lincs algorithm, respectively (37). After equilibration, the trajectories were recorded for 100 ns using the leap-frog algorithm (39).

Cell culture

The KYSE-30 esophageal cancer cell line was purchased from the Royan Institute (NCBI code: C584, Tehran, Iran). The cells were cultured in complete medium consisting of Dulbecco's modified Eagle medium (DMEM) with 10% fetal bovine serum (FBS; IdeaZist Co., Tehran, Iran) and 1% penicillin/streptomycin (Gibco, Life Technologies, USA). All cells were maintained in a humidified incubator at 37 ℃ with 5% CO_2, and the medium was replaced daily.

Cell viability assay

The 3-(4,5-dimethylthiazol-2-yl)-2,5-diphenyltetrazolium bromide (MTT) assay was used to determine cell viability treated with different concentrations of loratadine (40, 41). KYSE-30 cells were seeded at a density of 1 × 10^4 cells per well in a 96-well plate. The cells were then treated with different concentrations of loratadine (0, 1, 10, 25, 50, 75, 100, and 150 µM) compared to 0.6% Dimethyl Sulfoxide (DMSO) for 48 h. After treatment, 20 µL of MTT reagent (5 mg/mL) was added to each well, then the plate was incubated at 37 ℃ for 4 h. The medium was removed, and 100 µL of DMSO was added to dissolve the formazan crystals. The optical density (OD) of the solution was measured at a wavelength of 570 nm using a microplate reader. The results were compared to those obtained from the 0.6% DMSO vehicle group.

RNA Extraction

Total RNA was isolated using the RNX-PLUS kit (SINACLON, Tehran, Iran) according to the manufacturer's instructions. KYSE-30 cells were cultured in a T25 flask at a density of 1 × 10^6 cells and incubated for 48 h across three experimental groups:

loratadine group (cells treated with 100 µM loratadine); vehicle group (cells treated with 0.6% DMSO); and control group (cells without any treatment). Then, KYSE-30 cells were harvested using trypsin solution and washed twice with phosphate-buffered saline (PBS) buffer. RNA extraction was performed by lysing and homogenizing the cells with RNX-PLUS reagent at room temperature for 5 min. Chloroform was added to the samples, which were shaken vigorously for 5-10 s, and then incubated at room temperature for 15 min. The samples were centrifuged (12000 rpm, 15 min at 4 ℃), and the upper aqueous phase containing nucleic acids was carefully separated. The isolated RNA was precipitated by adding an equal volume of isopropanol, followed by incubation on ice for 15 min and then centrifugation. The RNA was washed by adding 1 mL of 75% ethanol, followed by centrifugation at 7500 rpm at 4 ℃ for 8 min (42). Finally, the purified RNA was resuspended in RNase-free water and stored at -80 ℃.

m6A ELISA assay

The m6A content in total RNA was quantified using an ELISA kit (m6A ELISA kit, Cat. No: ZB-15178c-H9648; Zell Bio GmbH, Germany) as previously described (43). Briefly, 1800 ng of RNA from each group was used to determine the m6A content. To eliminate all secondary structures in the RNA, the samples were heated at 95 ℃ for 5 min, followed by rapid cooling on ice. The denatured RNA was digested into nucleosides by incubating it with 4 units of nuclease P1 (Cat. No: Mo660s; BioLabs, USA) for 1 h at 37 ℃. Subsequently, 0.5 units of alkaline phosphatase (P0114; Sigma-Aldrich, Germany) and sufficient Tris buffer to achieve a final concentration of 100 mM Tris, pH 7.5, were added, and the mixture was incubated for 1 h at 37 °C. The supernatant was then collected and used for the ELISA assay. Absorbance was measured at a wavelength of 450 nm using a microplate reader. A standard curve was constructed to calculate the sample concentrations.

Statistical analysis

All statistical analyses were performed using GraphPad Prism version 8.4 (GraphPad Software, USA). The data are presented as the mean ± SD. Statistical significance was assessed using one-way ANOVA, followed by Tukey's post hoc test for comparisons involving more than two groups. P-values $\leq$ 0.05 were considered statistically significant. All experiments were conducted in triplicate or more.

RESULTS

Specific targeting

Blind docking is a useful method for discovering the binding sites of biological targets (44, 45). The regions of expected interactions between the 3DT (as the main ligand in the 3LFM crystallography structure) and FTO protein were identified by performing the molecular docking with AutoDock Tools 5.4. The binding pocket of the FTO protein (PDB ID: 3LFM) was predicted in the deepest cavity, which exists on chain A with a populated cluster and binding energy of -5.8 kcal/mol. The binding pocket residues were Glu234, Arg96, Tyr108, and Ser229. Our results are consistent with previous studies, which identified similar residues in the FTO binding pocket (46,47). The obtained results were visualized by BIOVINA Discovery Studio software (version 2021) (48) (Fig. 2).

Virtual screening and molecular docking

AutoDock Vina 1.2.3 was used for virtual screening over the library of the FDA-approved ZINC15 database, containing 1576 compounds docked on the defined FTO binding pocket to analyze molecular interactions and binding energy (49-51). Through the docking method, all compounds were compared, and the obtained results were sorted from lowest to highest binding energy. The top 50 compounds with the lowest binding energy were selected for further analysis, and all compounds were evaluated for their clinical applications. Some of the drugs, like peptides and chemotherapeutic medicines, were ignored. Also, compounds such as sunscreens, ointments, and creams were excluded from the study process. After applying these filters, the selected candidates were chosen for further investigation, as illustrated in Fig. 3, and their docking binding energies are demonstrated in Table 1.

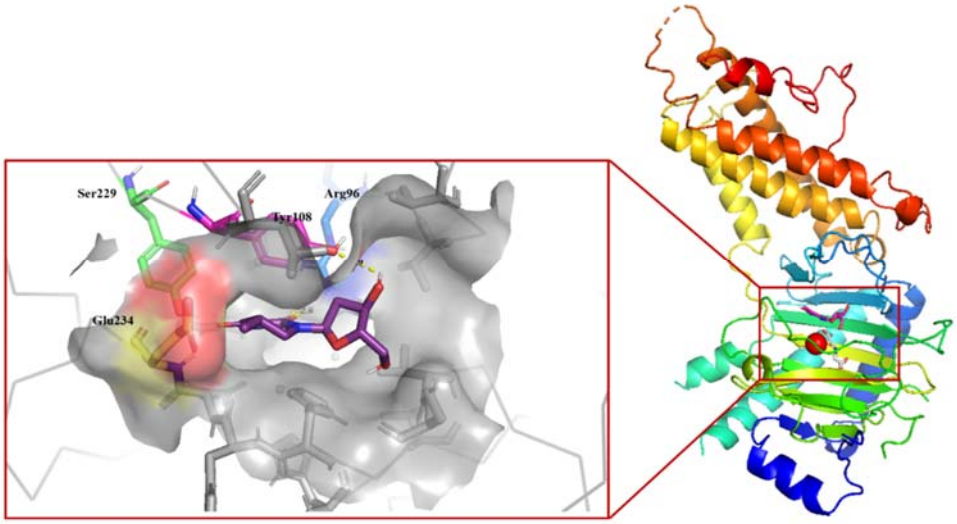

Fig. 2. The binding mode of 3DT on the groove area in the nucleotide binding site of the FTO protein. A schematic was generated using BIOVINA Discovery Studio software (version 2021). 3DT, 3-Methylthymidine; FTO, fat and obesity-associated protein.

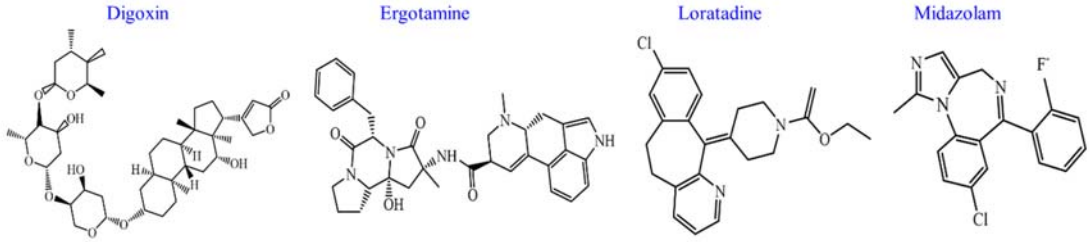

Fig. 3. The docking result produced the structures of the top four compounds. These structures were created using ChemDraw Ultra version 8.0, a chemical communication software program from PerkinElmer.

Table 1. Calculated binding energy and interactions of four docked compounds.

Zinc ID	General name	ΔG (Kcal/mol)	Estimated inhibition constant (Ki)	Residues of the action
ZINC242548690	Digoxin	-10.660	183.95 pM	Arg96, Arg80, Lys216, and Pro93
ZINC52955754	Ergotamine	-9.263	66.85 nM	Lys216, Tyr214, Val228, Leu90, and Val94
ZINC95626706	Midazolam	-8.904	1.29 µM	Asp233, Lue203, Val83, Ile85, and Thr92
ZINC537931	Loratadine	-8.900	1.06 µM	Val228, Lue109, Tyr108, His231, and Ser229
	3-Methylthymidine	-5.60	79.15 µM	Glu234, Arg96, Tyr108, and Ser229

The 3D structure of FTO with candidate ligands (digoxin, ergotamine, loratadine, and midazolam) was visualized using the PyMOL Molecular Graphics System (Fig. 4). In the case of digoxin, it binds to Arg96 and Arg80 *via* conventional hydrogen bonds. Digoxin binds to the Pro93 and Lys216 residues through the alkyl bond between the cyclohexane ring. Although the ergotamine compound did not form any hydrogen bonds with amino acid residues in the binding pocket, it formed pi-alkyl bonds with amino acid residues Lys216, Tyr214, Val228, Leu90, Val94, and Pro93 through the cyclohexadiene ring. Additionally, Lue90 residue has an alkyl interaction with the pyrroline ring of ergotamine.

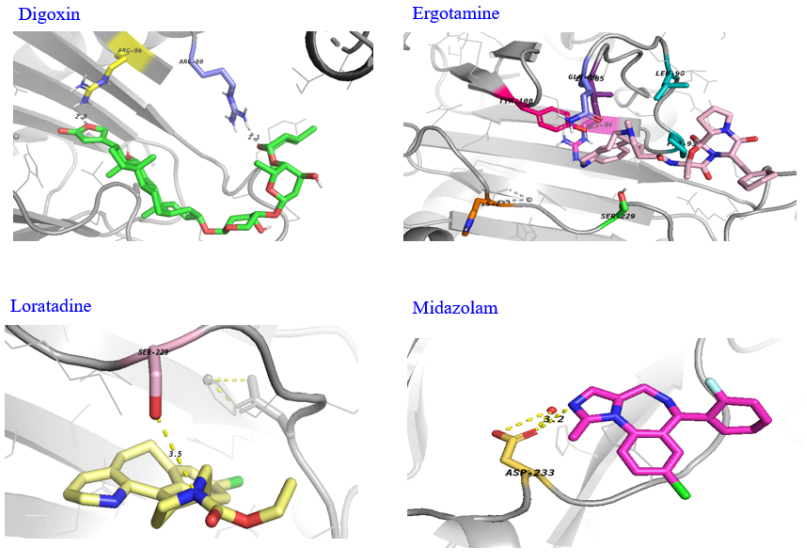

Fig. 4. Binding orientation of digoxin, ergotamine, loratadine, and midazolam and their interactions with the active site of the FTO protein. A schematic was generated using the PyMOL Molecular Graphics System version 1. Level Schrödinger, LLC. Available from https://pymol.org. FTO, fat and obesity-associated protein.

Besides, midazolam binds to the binding pocket amino acid residues through Asp233, Leu203, Ile80, Thr92, and Val83. Nitrogen within the pyrazine ring interacts with the hydrogen atom of the amine group. Furthermore, pi-alkyl interaction was established between the gamma carbon of Leu203 and the pyrazine ring. Moreover, the benzene ring of ergotamine interacted with the side chains of Val83 and Ile80 residues through a π-alkyl interaction. Similarly, a π-anion interaction was identified between the pyrazine ring and the radical oxygen donor of the Asp233 residue. As well, Thr92 has the pi-stacked interaction with the benzene ring

Moreover, a hydrogen bond was formed between the hydrogen of the hydroxyl group of the side chain of Ser229 with the nitrogen of the π-pyridine ring of loratadine. In addition, a pi-cation bond was established between the imidazole ring of His231 residue and the benzene ring in the loratadine structure. Furthermore, the benzene ring of loratadine established a π-π stacked bond with the phenolic ring of Tyr108 and a π-alkyl bond with the gamma carbon of Leu109. In the binding pocket of the FTO protein, it also established a hydrophobic π-alkyl and alkyl bond with the pyridine and cyclohexane ring in the structure of loratadine, respectively (52). The results are visualized in Fig. 5.

Estimated inhibition constant (Ki)

Moreover, to obtain the computationally estimated inhibition constant (Ki), we performed a docking analysis for four candidate compounds with the FTO protein crystallography structure using the molecular docking AutoDock Tools 1.5.7 (The Scripps Research Institute, La Jolla, CA, USA). The number of rotatable bonds of the ligand was set by default. However, if the number was greater than 6, some rotatable bonds were made nonrotatable; otherwise, calculations can be inaccurate. The active site was surrounded by a grid-box sized 70 × 70 × 70 points with a spacing of 0.375 Å. Ultimately, Ki value was determined for digoxin, ergotamine, loratadine, midazolam, and 3DT are shown in Table 1. Therefore, these results conclude that loratadine shows affinity for the FTO-binding pocket residues, and it could be considered an FTO inhibitor.

MD simulation

To determine the stability and behavior of the selected ligand, loratadine, in complex with the FTO, MD simulations were performed for 100 ns, and the analysis was carried out on its outputs (53). To compare output, we performed MD simulation for free FTO and FTO complex with specific ligand (3DT) bound to the FTO crystallographic structure (PDB ID: 3LFM) used in this study.

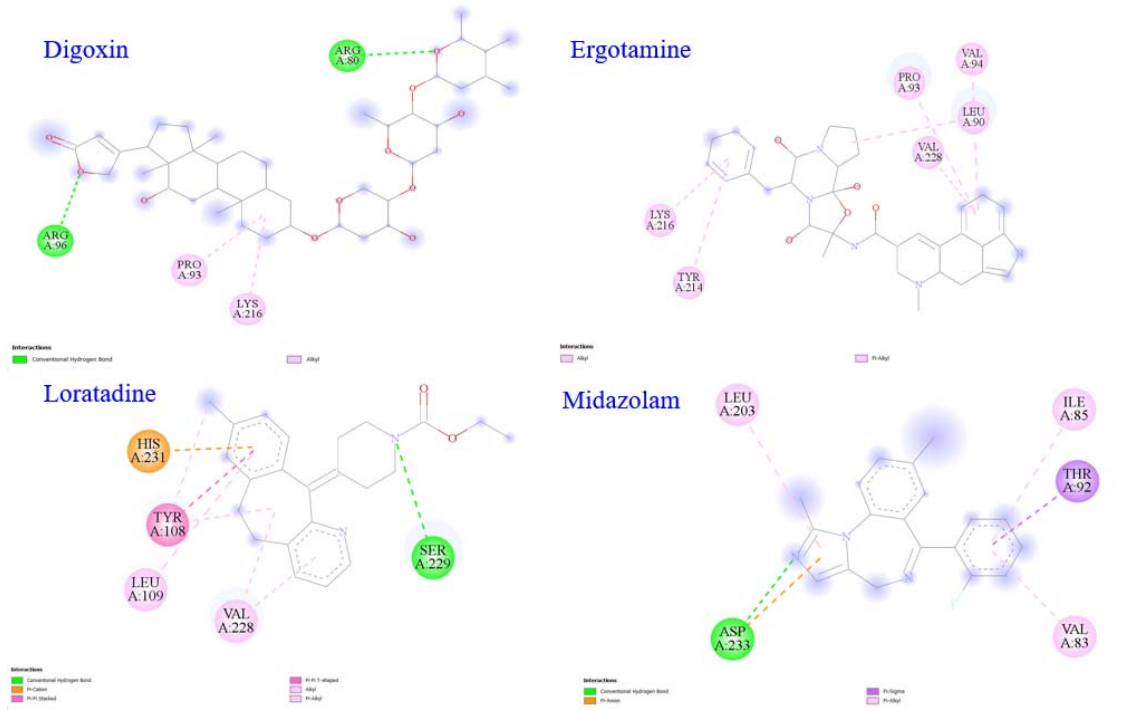

Fig. 5. 2D visualization of the interaction between digoxin, ergotamine, loratadine, and midazolam, with amino acid residues within the FTO (PDB ID: 3LFM) binding pocket generated by the BIOVINA Discovery Studio software. FTO, fat and obesity-associated protein.

The root mean square deviation (RMSD) is a metric that defines the deviation of a protein-ligand complex from the reference protein structure, with the RMSD value being measured (54-56). It was observed that the free FTO system fluctuations increased at 20 ns but were stable until the end of the MD simulation. Furthermore, the RMSD values of free FTO ranged from 0.3 to 0.5 nm, and the average RMSD value was 0.354 nm. Low RMSD fluctuations illustrated the stability until around 100 ns. Moreover, the FTO-3DT complex demonstrated a comparable RMSD with the reference protein up to 20 ns. However, beyond this timeframe, the complex experiences increased fluctuations, as evidenced by RMSD values ranging from 0.4 to 0.6 nm, and the average RMSD value was 0.522 nm. Moreover, the FTO-loratadine complex with 3DT as the reference ligand was analyzed. In the FTO-3DT complex, the average RMSD was 0.39, and its fluctuation was between 0.3 nm and 0.5 nm after 15 ns. Besides, the FTO-loratadine complex RMSD fluctuation was higher than the reference complex, but it was lower than the FTO-3DT complex. The RMSD plot is shown in Fig. 6A and B.

Then, to determine the deviation of each protein and amino acid residue concerning the reference position, the root mean square fluctuation (RMSF) plot (56) was calculated from 20 ns up to 100 ns MD trajectory as shown in Fig. 6C. The average values of RMSF for free FTO, FTO-loratadine, and FTO-3DT complexes were approximately 0.123, 0.125, and 0.136 nm, respectively. Interestingly, it was declared that the RMSF values of the FTO-loratadine complex exhibited an overall similar and slightly higher RMSF value when compared with the free FTO protein during the simulation time between 20 and 100 ns. In addition, the RMSF value of the FTO-loratadine complex was lower than the FTO-3DT RMSF value. Additionally, the overall 100 ns timescale of the MD simulation revealed that the average values of total RMSF for free FTO, FTO-loratadine, and FTO-3DT complexes are 0.152, 0.187, and 0.192 nm, respectively. This finding means that the FTO-loratadine complex has more fluctuation compared to free FTO but

is lower than the FTO-3DT complex, indicating that the structure was defined as suitable. Furthermore, in the 100 ns timescale of RMSF, Tyr108, Leu109, Val228, and His231 amino acid residues in free FTO are 0.121, 0.099, 0.131, and 0.11 nm, respectively. Furthermore, the RMSFs of these amino acid residues in the FTO-loratadine complex system are 0.166, 0.145, 0.191, and 0.167 nm, respectively. The RMSF results demonstrated that both the free protein and the protein-ligand complex have regions with similar degrees of flexibility. The FTO-loratadine complex tended to exhibit slightly higher average fluctuations, indicating that the presence of the ligand may affect the dynamic behavior of the protein.

The compactness and rigidity of the free FTO protein and FTO-loratadine complex were investigated using the Radius of gyration (Rg). The average Rg values of free FTO, FTO-loratadine, and FTO-3DT complexes were 2.554, 2.564, and 2.547, respectively. The average Rg values revealed that the free protein and complexes have comparable compactness. The results obtained from the Rg profile indicated that the FTO-loratadine complex, along with the reference protein and FTO-3DT complex, remained stable between 2.5 and 2.65 nm throughout the 100 ns timescale. The stability observed in the Rg profile between 2.49 and 2.65 nm indicates that overall, the structures maintain a relatively consistent level of compactness. The fluctuations generated at the beginning of the MD for the free protein and the complex are probably due to adaptation to the system. The results are illustrated in Fig. 6D.

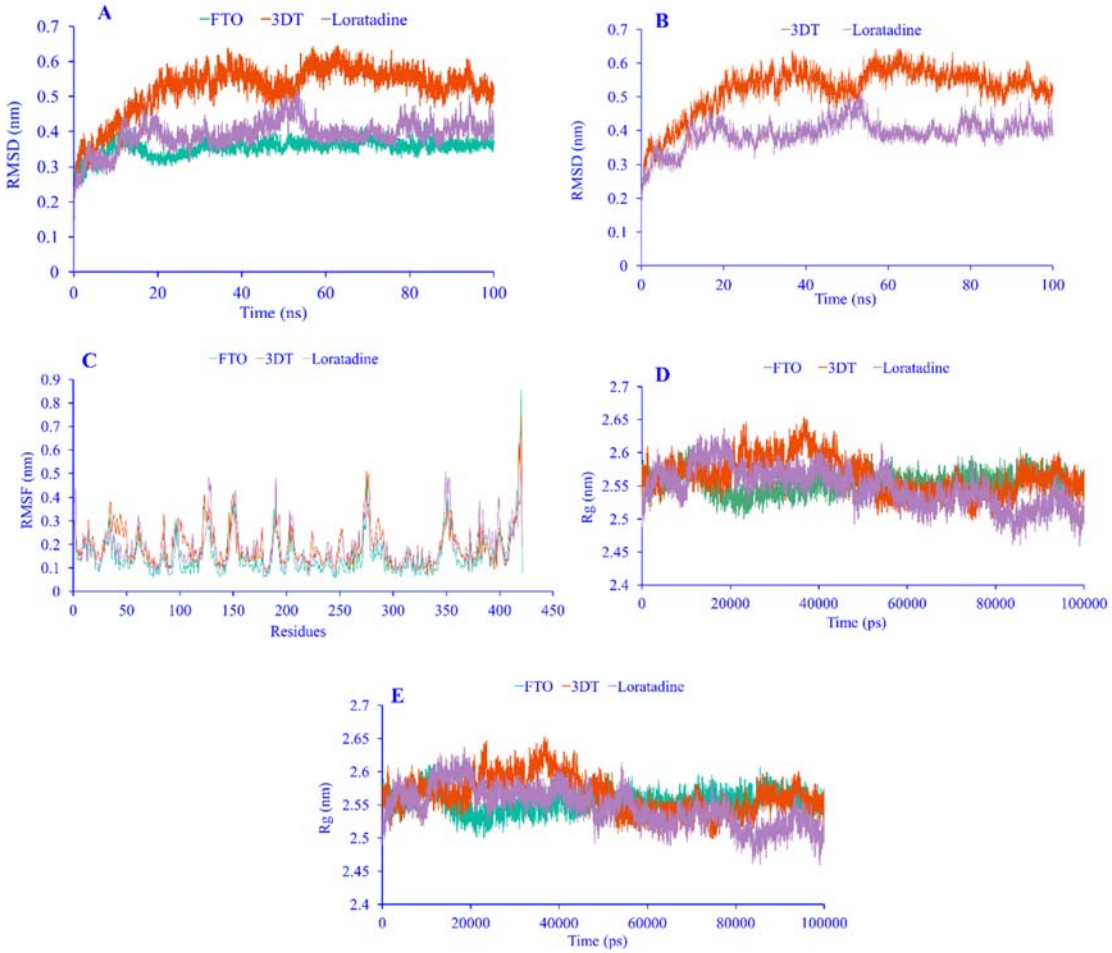

Fig. 6. Superimposed (A) RMSD, (B) ligands RMSD, (C) RMSF, (D) Rg, and (E) SASA plots. Green represents the free FTO system; red for the FTO-3DT complex, and purple represents the FTO-loratadine complex. RMSD, Root mean square deviation; RMSF, root mean square fluctuation; Rg, radius of gyration; SASA, solvent accessible surface area; FTO, fat and obesity-associated protein; 3DT, 3-methylthymidine.

To investigate protein surface area and folding, we analyzed the solvent accessible surface area (SASA) plot for each system, which was constructed from the protein trajectory (57). The SASA results aid in determining whether the ligand remains within the binding pocket or is expelled from the cavity. The average SASA values for free FTO, FTO-loratadine, and FTO-3DT complexes were 219.516, 218.413, and 216.464 nm, respectively. The obtained results are illustrated in Fig. 6E. The analysis of SASA provides insights into the ligand's interaction with the binding pocket. The small difference in average SASA between the free protein and the complexes indicated the minimal changes in the overall surface accessibility upon ligand binding.

Hydrogen bond formation is the necessary driving force that specifies stability and ligand specificity (57, 58). Analysis of the main FTO-loratadine complex demonstrated that loratadine forms a hydrogen bond with the binding pocket amino acid residues. To analyze the hydrogen bond interaction property during the 100 ns period of simulation, the hydrogen bond interaction plot was constructed. The number of hydrogen bonds formed in the FTO-loratadine complex is approximately twice that of the hydrogen bonds formed in the FTO-3DT complex. The number of hydrogen bonds of FTO-3DT and FTO-loratadine complex is demonstrated in Fig. 7A and B.

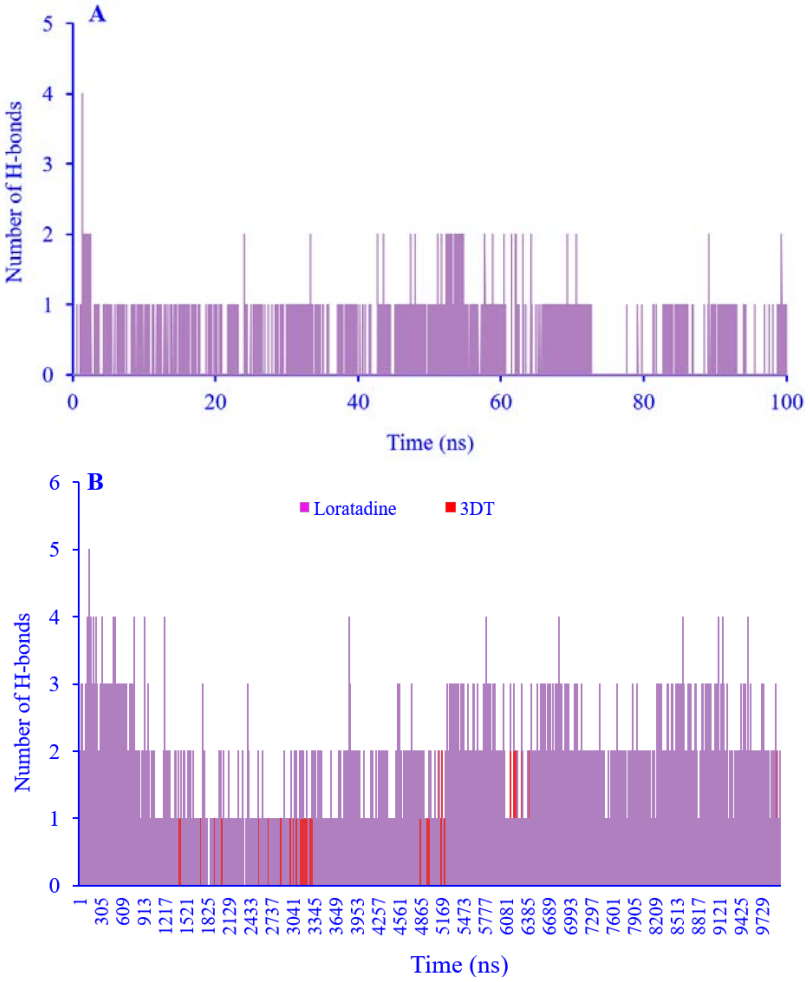

Fig. 7. H-bonds were observed between (A) FTO and loratadine, and (B) between FTO with 3DT and loratadine during the molecular dynamic simulation. The symbol coding scheme is as follows: FTO-loratadine (purple) and FTO-3DT (red). H-bond, Hydrogen bond; FTO, fat and obesity-associated protein; 3DT, 3-methylthymidine.

Binding free energy calculations

To analyze the binding of ligand-protein complexes in dynamic simulations, the molecular mechanics Poisson-Boltzmann surface area (MM/PBSA) approach was used to compute the binding free energy. This method contributed to the calculation of various energy components, including electrostatic energy, polar solvation energy, SASA, and van der Waals (Vdw) energy. The results obtained from MM/PBSA for both FTO-3DT and FTO-loratadine complexes are illustrated in Table 2.

The MM/PBSA (Molecular Mechanics/ Poisson-Boltzmann Surface Area) calculations for the FTO-loratadine and FTO-3DT complexes provide valuable insights into the binding energetics of these compounds to the FTO receptor. The ΔG binding energy was computed by evaluating various energies, including van der Waals (ΔG Vdw), electrostatic (ΔG elec), polar solvation (ΔG polar), and SASA (ΔG SASA) energies.

Both complexes exhibited negative binding energies, indicating a favorable binding between the receptor and the ligands. Specifically, the ΔG binding energy for loratadine was -135.73 ± 17.15 kJ/mol, while for 3DT, it was -104.68 ± 11.12 kJ/mol. These negative values suggest that both compounds have a suitable binding affinity to the FTO receptor, while loratadine shows a stronger binding affinity compared to 3DT as the main ligand in the FTO crystallography structure.

The ΔG Vdw and ΔG elec contributions play a significant role in determining the overall binding energy. For both ligands, the ΔG Vdw was highly negative, indicating that the favorable interactions between the ligands and the receptor. Loratadine demonstrated a more negative van der Waals energy (-185.97 ± 9.75 kJ/mol) compared to 3DT (-152.91 ± 10.52 kJ/mol), which offers stronger van der Waals interactions for loratadine. The ΔG elec for 3DT (-21.56 ± 6.74 kJ/mol) was more negative than for loratadine (-1.51 ± 3.59 kJ/mol), suggesting that electrostatic interactions play a more critical role in the binding of 3DT. These favorable van der Waals interactions further contributed to the overall binding affinity of both compounds.

Moreover, the positive polar ΔG values for both complexes suggest a solvent release cost upon binding. Specifically, the polar solvation energy for loratadine was 71.99 ± 14.28 kJ/mol, while for 3DT, it was 84.08 ± 10.37 kJ/mol. This positive contribution suggests that the binding process is energetically costly for desolvation of the ligand and receptor in a polar environment (e.g., water). While this desolvation cost is not ideal, it is a common part of protein-ligand interactions, where the ligand and receptor need to lose their surrounding water molecules to bind. Although the positive polar solvation energies are unfavorable, they do not diminish the overall favorable binding energy, including van der Waals and electrostatic interactions, which are highly favorable and offset this cost.

The non-polar solvation energy (ΔG SASA), which reflects the desolvation of the non-polar surface area, was negative for both complexes, which offers a favorable contribution to binding. Loratadine has a more negative ΔG SASA (-20.23 ± 0.77 kJ/mol) compared to 3DT (-14.28 ± 0.72 kJ/mol), which suggests that the desolvation of the non-polar surface area around loratadine is more energetically favorable than for 3DT.

Cell viability

We used the MTT assay to determine the toxicity of loratadine on the KYSE-30 cell line for 48 h. The obtained results illustrated those various concentrations of loratadine, except for 150 μM, had no cytotoxic effect on the KYSE-30 cell line compared to the vehicle group (DMSO, 0.6%). Our findings showed that higher concentrations of loratadine, above 150 μM, could reduce the viability of KYSE-30 cells in a concentration-dependent manner. Subsequently, we selected a 100 μM concentration of loratadine as the highest concentration, which was not toxic to the KYSE-30 cells but could cause changes in the m6A level during the treatment process. The obtained results are demonstrated in Fig. 8A.

Table 2. MM/PBSA energy results for FTO-3DT and FTO-loratadine complexes.

Compound	ΔG binding energy (kcal/mol)	ΔG Vdw (kcal/mol)	ΔG elec (kcal/mol)	ΔG polar (kcal/mol)	ΔG SASA (kcal/mol)
Loratadine	-135.73 ± 17.15	-185.97 ± 9.75	-1.51 ± 3.59	71.99 ± 14.28	-20.23 ± 0.77
3DT	-104.68 ± 11.12	-152.91 ± 10.52	-21.56 ± 6.74	84.08 ± 10.37	-14.28 ± 0.72

FTO, fat and obesity-associated protein; 3DT, 3-methylthymidine; Vdw, van der Waals; elec, electrostatic; polar solvation (ΔG polar), SASA, solvent accessible surface area

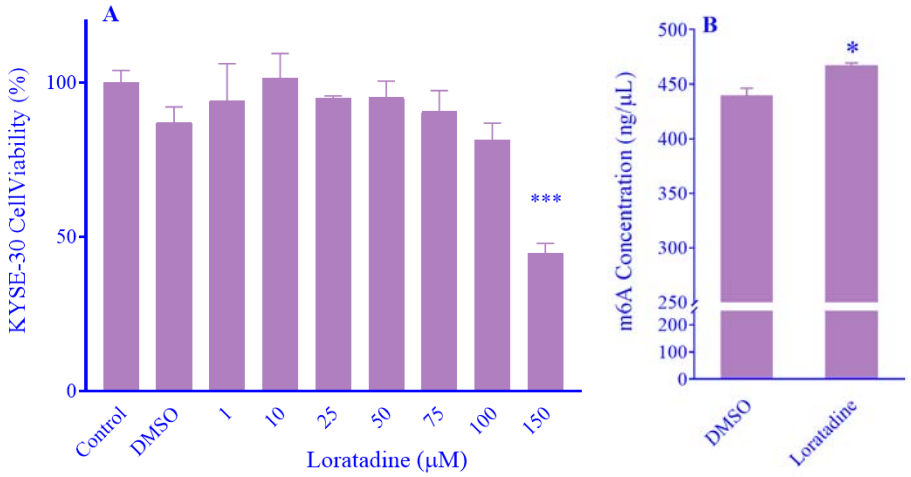

Fig. 8. (A) Cytotoxic effect evaluation of various concentrations of loratadine on KYSE-30 cells after 48-h treatment using the MTT assay; (B) m6A level in total RNA isolated from KYSE-30 cells treated with loratadine (100 µM) or DMSO 0.6%. $P \leq 0.05$ and $P \leq 0.001$ indicate significant differences compared to DMSO 0.6%.

m6A levels in total RNA isolated from the KYSE-30 cell line

The previous studies suggest that the suppression of FTO may lead to an increase in m6A content within RNA (16, 17, 59). To confirm this hypothesis, the ELISA assay was utilized. For this purpose, KYSE-30 cells were treated with 100 µM of loratadine alongside 0.6% DMSO as a control. The findings revealed that after 48 h of treatment with loratadine at 100 µM, there was a significant elevation in m6A levels in the total RNA when compared to the DMSO control group (Fig. 8B).

DISCUSSION

This study explored FDA-approved drugs as potential FTO inhibitors, an m6A demethylase linked to obesity, diabetes (60), cardiovascular diseases (61), and cancers (*e.g.*, esophageal cancer) (62). FTO regulates key metabolic and developmental processes (glucose/fat metabolism, growth, fertility) by removing m6A marks from mRNAs in the epitranscriptome (63-68). Therefore, its inhibition may be an appropriate target for the treatment of FTO-dependent diseases.

MD identified ergotamine, loratadine, midazolam, and digoxin as interactors with FTO's binding pocket. Loratadine (a second-generation antihistamine used for allergies) emerged as the most promising FTO inhibitor due to its favorable binding profile (69, 70). MD simulation revealed loratadine's strong FTO binding *via* (1) stable complex formation, (2) maintaining hydrogen bonds, and (3) favorable energies. These computational results strongly suggest that loratadine could effectively inhibit FTO's m6A demethylase activity, making it a prime candidate for further drug development targeting RNA epigenetic modifications. Several studies have focused on FTO inhibitors; however, more investigation is needed on the FDA-approved drugs approach to drug repurposing (51, 60, 71-74). Notable studies by Huang *et al*. (75), Wang *et al*. (76), Peng *et al*. (77), and Han *et al.* (78) have identified meclofenamic acid, fluorescein, entacapone, and nafamostat mesylate,

respectively, as potential FDA-approved FTO inhibitors.

Huang *et al*. demonstrated that meclofenamic acid and its derivative (ethyl ester-MA, MA2) effectively inhibit the m6A demethylase activity of FTO. Their study established a safe dosage range for MA2 between 80-120 µM. Notably, our findings indicated that loratadine exhibits comparable inhibitory effects at concentrations below 100 µM, suggesting potentially greater inhibitory potency against FTO's m6A demethylase activity at lower concentrations (75). Additionally, Wang *et al*. identified fluorescein (FL) derivatives as potent FTO inhibitors and binding ligands. Treatment with FL8 and FL9 at concentrations ranging from 20 to 150 µM resulted in cell viabilities exceeding 95%, indicating low cytotoxicity. However, this level of viability was relatively lower than the established safety profile observed with loratadine. Although fluorescein derivatives exhibited favorable cytotoxicity profiles, they are primarily advantageous for FTO labeling applications rather than therapeutic inhibition (76).

Furthermore, Peng *et al*. demonstrated that entacapone effectively inhibits FTO demethylase activity, resulting in elevated m6A levels in HepG2 cells at concentrations of 10-100 µM, a range comparable to our observations with loratadine. This functional similarity likely stems from shared structural features between these compounds that facilitate analogous binding interactions with FTO's binding site (77).

FTO-04 compound has been reported to considerably increase m6A levels in glioblastoma stem cells through FTO inhibition at a low concentration of 2.79 µM, which is inconsistent with our observations. Loratadine required a higher concentration (100 µM) to achieve comparable effects. This differential potency may be attributed to both structural variations between the compounds and inherent differences in cell line sensitivity to treatment (79). Subsequently, our findings revealed that loratadine has inhibitory potential on FTO demethylase activity, which increases m6A levels in RNA isolated from KYSE-30 cells treated with loratadine at 100 µM.

This study computationally identified loratadine as a promising FDA-approved FTO inhibitor, demonstrating stable binding and potential epigenetic modulation at concentrations less than 100 µM. While existing inhibitors (*e.g.*, MA2, entacapone, FTO-04) show variable potency across cell lines, loratadine's balanced efficacy and safety profile position it as a viable candidate for repurposing against FTO-related diseases. Further experimental validation is warranted to establish its therapeutic potential relative to known inhibitors.

CONCLUSION

FDA-approved virtual screening of 1576 drugs was performed over the FTO-binding pocket. The virtual screening consisted of four ligands, including midazolam, ergotamine, digoxin, and loratadine. MD simulation applied to determine the stability of loratadine as the selected ligand in the FTO-binding pocket for 100 ns. MD simulation results were also in good agreement with docking results and revealed the appropriate stability along with proper interaction during 100 ns, for loratadine. Besides, the *in vitro* study confirmed that FTO inhibition by loratadine led to an increase in the m6A levels in total RNA isolated from the KYSE-30 esophageal cancer cell line.

Acknowledgments

This work was financially supported by the Research Committee of Golestan University of Medical Sciences through Grant No. IR.GOUMS.REC.1401.301. We would like to thank Golestan University of Medical Sciences and Tehran University of Medical Sciences for their support and assistance throughout this study.

Conflict of interest statement

The authors declared no conflict of interest in this study.

Author's contribution

J. Asadi and M. Saghaeian Jazidesigned and supervised the study. M. Amanlou was the consultant for the *in silico* tests and analysis of the results. S.M. Jafari was the consultant for experimental tests. Z. Mohammadi performed *in*

silico studies, experimental tests and analyzed the results. Additionally, Z. Mohammadi, S. Saghaeian Jazi, S.M. Jafari, M. Amanlou and S.M. Mir wrote the article. All authors read and approved the final version of the article.

REFERENCE

1. Maity A, Das B. N6-methyladenosine modification in mRNA: machinery, function and implications for health and diseases. FEBS J. 2016;283(9):1607-1630. DOI: 10.1111/febs.13614.
2. Roundtree IA, Evans. ME, Pan T, He C. Dynamic RNA modifications in gene expression regulation. Cell. 2017;169(7):1187-1200. DOI: 10.1016/j.cell.2017.05.045.
3. Brown JA, Kinzig CG, DeGregorio SJ, Steitz JA. Methyltransferase-like protein 16 binds the 3′-terminal triple helix of MALAT1 long noncoding RNA. Proc Nati Acad Sci. 2016;113(49):14013-14018. DOI: 10.1073/pnas.1614759113.
4. Liu J, Yue Y, Han D, Wang X, Fu Y, Zhang L, *et al*. A METTL3–METTL14 complex mediates mammalian nuclear RNA n6-adenosine methylation. Nat Chem Biol. 2014;10(2):93-95. DOI: 10.1038/nchembio.1432.
5. Meyer KD, Jaffrey SR. Rethinking m6a readers, writers, and erasers. Annu Rev Cell Dev Biol. 2017;33(1):319-342. DOI: 10.1146/annurev-cellbio-100616-060758.
6. Jia G, Fu Y, Zhao X, Dai Q, Zheng G, Yang Y, *et al*. N6-methyladenosine in nuclear RNA is a major substrate of the obesity-associated FTO. Nat Chem Biol. 2011;7(12):885-887. DOI: 10.1038/nchembio.687.
7. Zheng G, Dahl JA, Niu. Y, Fedorcsak P, Huang CM, Li CJ, *et al*. ALKBH5 is a mammalian RNA demethylase that impacts RNA metabolism and mouse fertility. Mol Cell. 2013;49(1):18-29. DOI: 10.1016/j.molcel.2012.10.015.
8. Wang J, Wang J, Gu Q, Ma Y, Yang Y, Zhu J, *et al*. The biological function of m6a demethylase alkbh5 and its role in human disease. Cancer Cell Int. 2020;20(1):347,1-7. DOI: 10.1186/s12935-020-01450-1.
9. Wojtaz. M. Pandey RR, Mendel. M, Homolka D, Sachidanandam R, Pillai RS. Regulation of m6A transcripts by the 3'→5' RNA helicase YTHDC2 is essential for a successful meiotic program in the mammalian germline. Mol Cell. 2017;68(2):374-387. DOI: 10.1016/j.molcel.2017.09.021.
10. Dina C, Meyre D, Gallina S, Durand E, Körner A, Jacobson P, *et al*. Variation in FTO contributes to childhood obesity and severe adult obesity. Nat Genet. 2007;39(6):724-726. DOI: 10.1038/ng2048.
11. Zhao X, Yang Y, Sun BF, Zhao YL, Yang YG. FTO and obesity: mechanisms of association. Curr Diab Rep. 2014;14(5):486,1-9. DOI: 10.1007/s11892-014-0486-0.
12. Qing Y, Dong L, Gao L, Li C, Li Y, Han L, *et al*. R-2-hydroxyglutarate attenuates aerobic glycolysis in leukemia by targeting the fto/m6a/pfkp/ldhb axis. Mol Cell. 2021;81(5):922-939.e9. DOI: 10.1016/j.molcel.2020.12.026.
13. Wang L, Song C, Wang N, Li S, Liu Q, Sun Z, *et al*. NADP modulates RNA m6a methylation and adipogenesis via enhancing FTO activity. Nat Chem Biol. 2020;16(12):1394-1402. DOI: 10.1038/s41589-020-0601-2.
14. Xiang Y, Laurent B, Hsu CH, Nachtergaele S, Lu Z, Sheng W, *et al*. RNA m6a methylation regulates the ultraviolet-induced DNA damage response. Nature. 2017;543(7646):573-5766. DOI: 10.1038/nature21671.
15. Smemo S, Tena JJ, Kim KH, Gamazon ER, Sakabe NJ, Gómez-Marín C, *et al*. Obesity-associated variants within FTO form long-range functional connections with irx3. Nature. 2014;507(7492):371-375. DOI: 10.1038/nature13138.
16. Su R, Dong L, Li C, Nachtergaele S, Wunderlich M, Qing Y, *et al*. R-2HG exhibits anti-tumor activity by targeting FTO/m6A/MYC/CEBPA Signaling. Cell. 2018;172(1-2):90-105.e23. DOI: 10.1016/j.cell.2017.11.031.
17. Duan X, Yang L, Wang L, Liu Q, Zhang K, Liu S, *et al*. M6a demethylase FTO promotes tumor progression via regulation of lipid metabolism in esophageal cancer. Cell Biosci. 2022;12(1):60,1-14. DOI: 10.1186/s13578-022-00798-3.
18. Cui Y, Zhang C, Ma S, Li Z, Wang W, Li Y, *et al*. RNA m6a demethylase FTO-mediated epigenetic up-regulation of linc00022 promotes tumorigenesis in esophageal squamous cell carcinoma. J Exp Clin Cancer Res. 2021;40(1):294,1-20. DOI: 10.1186/s13046-021-02096-1.
19. Liu S, Huang M, Chen Z, Chen J, Chao Q, Yin X, Quan M. FTO promotes cell proliferation and migration in esophageal squamous cell carcinoma through up-regulation of MMP13. Exp Cell Res. 2020;389(1),111894,1-8. DOI: 10.1016/j.yexcr.2020.111894.
20. B. Singh, Kinne HE, Milligan RD, Washburn LJ, Olsen M, Lucci A. Important role of FTO in the survival of rare panresistant triple-negative inflammatory breast cancer cells facing a severe metabolic challenge. PLoS One 2016;11(7),1-20. DOI: 10.1371/journal.pone.0159072.
21. Tan NN, Tang HL, Lin GW, Chen YH, Lu P, Li HJ, *et al*. Epigenetic downregulation of Scn3a expression by valproate: a possible role in its anticonvulsant activity. Mol Neurobiol. 2017;54(4):2831-2842. DOI: 10.1007/s12035-016-9871-9.
22. Toh JDW, Sun L, Lau LZM, Tan J, Low JJA, Tang CWQ, *et al*. A strategy based on nucleotide specificity leads to a subfamily-selective and cell-active inhibitor of n6-methyladenosine demethylase FTO. Chem Sci. 2015;6:112-122. DOI: 10.1039/c4sc02554g.
23. Padariya M, KalathiaU. Structure-based design and evaluation of novel n-phenyl-1H-indol-2-amine derivatives for fat mass and obesity-associated (FTO) protein inhibition. Comput Biol Chem. 2016;64:414-425.

DOI: 10.1016/j.compbiolchem.2016.09.008.
24. Rui S, Dong L, Li Y, Gao M, Han L, Wanderlich M, *et al.* Targeting FTO suppresses cancer stem cell maintenance and immune evasion. Cancer Cell. 2020;38(1):79-96. DOI: 10.1016/j.ccell.2020.04.017.
25. He W, Zhou B, Liu W, Zhang M, Shen Z, Han Z, *et al*. Identification of a novel small-molecule binding site of the fat mass and obesity associated protein (FTO). J Med Chem. 2015;58(18):7341-7348. DOI: 10.1021/acs.jmedchem.5b00702.
26. Alimardan Z, Abbasi M, Khodarahmi G, Kashfi K, Hasanzadeh F, Mahmud A. Identification of new small molecules as dual Foxm1 and hsp70 inhibitors using computational methods. Res Pharm Sci. 2022;17(6):635-656. DOI: 10.4103/1735-5362.359431.
27. Pushpakom S, Iorio F, Eyers PA, Escott KJ, Hopper S, Wells A, *et al*. Drug repurposing: progress, challenges and recommendations. Nat Rev Drug Discov. 2019;18(1):41-58. DOI: 10.1038/nrd.2018.168.
28. Morris GM, Huey R, Lindstrom W, Sanner MF, Belew RK, Goodsell DS, *et al*. Autodock4 and autodocktools4: automated docking with selective receptor flexibility. J Comput Chem. 2009;30(16):2785-2791. DOI: 10.1002/jcc.21256.
29. Azizian HN, Nabati F, Sharifi A, Siavoshi F, Mahdavi M. Amanlou, M. Large-scale virtual screening for the identification of new *Helicobacter pylori* urease inhibitor scaffolds. J Mol Model. 2012;18(7):2917-2927. DOI: 10.1007/s00894-011-1310-2.
30. Trott O, Olson AJ. Autodock vina: improving the speed and accuracy of docking with a new scoring function, efficient optimization, and multithreading. J Comput Chem. 2010;31(2):455-461. DOI: 10.1002/jcc.21334.
31. O'Boyle NM, Banck M, James CA, Morley C, Vandermeersch T, Hutchison GR."Open babel: An open chemical toolbox." J Cheminf. 2011;3:33,1-14. DOI: 10.1186/1758-2946-3-33.
32. Lindahl A, Hess, & van der Spoel. Gromacs 2021 manual (version 2021). Zenodo 2021. DOI: 10.5281/zenodo.4457591.
33. Der Spoel DV, Lindahl E, Hess B, Groenhof G, Mark AE, Berendsen HJ. Gromacs: fast, flexible, and free. J Comput Chem. 2005;26(16):1701-1718. DOI: 10.1002/jcc.20291.
34. Nosé S, Klein ML. Constant pressure molecular dynamics for molecular systems. Mol Phys. 1983;50(5):1055-1076. DOI: 10.1080/00268978300102851.
35. Nosé S. A molecular dynamics method for simulations in the canonical ensemble. Mol Phys. 1984;52(2):255-268. DOI: 10.1080/00268978400101201.
36. Hoover WG. Canonical dynamics: equilibrium phase-space distributions. Phys Rev A Gen Phys 1985;31(3):1695-1697. DOI: 10.1103/physreva.31.1695.
37. Berendsen HJC, Postma JPM, van Gunsteren WF, DiNola A, Haak JR. Molecular dynamics with coupling to an external bath. J Chem Phys. 1984;81:3684-3690. DOI: 10.1063/1.448118.
38. Beutler TC, Van Gunsteren WF. Molecular dynamics simulations with first-order coupling to a bath of constant chemical potential. Molecular Simulation. 1994;14(1):21-34. DOI: 10.1080/08927029408022005.
39. Essmann U, Perera L, Berkowitz ML, Darden T, Lee H, Pedersen LG. A smooth particle mesh ewald method. J Chem Phys. 1995;103(19):8577-8593. DOI: 10.1063/1.470117.
40. van Meerloo J, Kaspers GJ, Cloos J. Cell sensitivity assays: the MTT assay. Methods Mol Biol. 2011;731:237-245. DOI: 10.1007/978-1-61779-080-5_20.
41. Taghvaei F, Rastin SJ, Milani AT, Khameneh ZR, Hamini F, Rasouli MA, *et al*. Carboplatin and epigallocatechin-3-gallate synergistically induce cytotoxic effects in esophageal cancer cells. Res Pharm Sci. 2021;16(3):240-249. DOI: 10.4103/1735-5362.314822.
42. Rio DC, Ares Jr M, Hannon GJ, Nilsen TW. Purification of RNA using TRIzol (TRI reagent). Cold Spring Harbor Protoc. 2010;2010(6):1-70. DOI: 10.1101/pdb.prot5439.
43. Ramedani F, Jafari SM, Saghaeian Jazi M, Mohammadi Z, Asadi J. Anti-cancer effect of entacapone on esophageal cancer cells via apoptosis induction and cell cycle modulation. Cancer Reports (Hoboken, NJ). 2023;6(3):e1759,1-8. DOI: 10.1002/cnr2.1759.
44. Iorga B, Herlem D, Barré E, Guillou C. Acetylcholine nicotinic receptors: finding the putative binding site of allosteric modulators using the "blind docking" approach. J Mol Model. 2006;12(3):366-372. DOI: 10.1007/s00894-005-0057-z.
45. Hetényi C, van der Spoel D. Blind docking of drug-sized compounds to proteins with up to a thousand residues. FEBS Lett 2006;580(5):1447-1450. DOI: 10.1016/j.febslet.2006.01.074.
46. You Y, Fu Y, Huang M, Shen D, Zhao B, Liu H, *et al*. Recent advances of m6A demethylases inhibitors and their biological functions in human diseases. Int J Mol Sci. 2022;23(10):1-28. DOI: 10.3390/ijms23105815.
47. Han Z, Niu T, Chang J, Lei X, Zhao M, Wang Q, *et al*. Crystal structure of the FTO protein reveals basis for its substrate specificity. Nature. 2010;464(7292):1205-1209. DOI: 10.1038/nature08921.
48. Li Q, Huang Y, Liu X, Gan J, Chen H, Yang CG. Rhein inhibits AlkB repair enzymes and sensitizes cells to methylated DNA damage. J Biol Chem. 2016;291(21):11083-11093. DOI: 10.1074/jbc.M115.711895.
49. Trott O, Olsen AJ. AutoDock Vina: improving the speed and accuracy of docking with a new scoring function, efficient optimization and multithreading. J Comput Chem. 2010;31(2): 455-461.

DOI: 10.1002/jcc.21334.
50. Jaghoori MM, Bleijlevens B, Olabarriaga SD. 1001 ways to run autodock vina for virtual screening. J Comput Aided Mol Des. 2016;30(3):237-249. DOI: 10.1007/s10822-016-9900-9.
51. Wang RY, Han ZF, Liu BJ, Zhou B, Wang N, Jiang QW, *et al*. Identification of natural compound radicicol as a potent FTO inhibitor. Mol Pharm. 2018;15(9):4092-4098. DOI: 10.1021/acs.molpharmaceut.8b00522.
52. Li H, Song Y, He Z, Chen X, Wu X, Li X, *et al*. Meclofenamic acid reduces reactive oxygen species accumulation and apoptosis, inhibits excessive autophagy, and protects hair cell-like HEI-OC1 cells from cisplatin-induced damage. Front Cell Neurosci. 2018;12:139,1-12. DOI: 10.3389/fncel.2018.00139.
53. Hashemi S, Sharifi A, Zareei S, Mohamedi G, Biglar M, Amanlou M. Discovery of direct inhibitor of KRAS oncogenic protein by natural products: a combination of pharmacophore search, molecular docking, and molecular dynamic studies. Res Pharm Sci. 2020;15(3):226-240. DOI: 10.4103/1735-5362.288425.
54. Sargsyan K, Grauffel C, Lim C. How molecular size impacts RMSD applications in molecular dynamics simulations. J Chem Theory Comput. 2017;13(4):1518-1524. DOI: 10.1021/acs.jctc.7b00028.
55. Knapp B, Frantal S, Cibena M, Schreiner W, Bauer P. Is an intuitive convergence definition of molecular dynamics simulations solely based on the root mean square deviation possible? J Comput Biol. 2011;18(8):997-1005. DOI: 10.1089/cmb.2010.0237.
56. Berger MB, Walker AR, Montelongo EA, Cisneros GA. Computational investigations of selected enzymes from two iron and α-ketoglutarate-dependent families. Physi Chem Chem Phys. 2021;39:1-16. DOI: 10.48550/arXiv.2108.10959.
57. Kumar SU, Rajan B, Kumar DT, Cathryn RH, Das Sth S, Zayed H, *et al*. Comparison of potential inhibitors and targeting fat mass and obesity-associated protein causing diabesity through docking and molecular dynamics strategies. J Cell Biochem. 2021:122(11):1625-1638. DOI: 10.1002/jcb.30109.
58. Bopp P. Molecular dynamics computer simulations of solvation in hydrogen bonded systems. Pure App Chem. 1987;59(9):1071-1082.
59. Li Z, Weng H, Su R, Weng X, Zuo Z, Li C, *et al*. FTO plays an oncogenic role in acute myeloid leukemia as a n6-methyladenosine RNA demethylase. Cancer cell. 2017;31(1):127-141. DOI: 10.1016/j.ccell.2016.11.017.
60. Qiao Y, Zhou B, Zhang MZ, Liu WJ, Han ZF, Song CJ, *et al*. A novel inhibitor of the obesity-related protein FTO. Biochemistry. 2016;55(10):1516-1522. DOI: 10.1021/acs.biochem.6b00023.
61. Hotta K, Kitamoto T, Kitamoto A, Mizusawa S, Matsuo T, Nakata Y, *et al*. Association of variations in the FTO, SCG3 and MTMR9 genes with metabolic syndrome in a Japanese population. J Hum Genet. 2011;56(9):647-651. DOI: 10.1038/jhg.2011.74.
62. Qin B, Bai Q, Yan D, Yin F, Zhu Z, Xia C, *et al*. Discovery of novel mRNA demethylase FTO inhibitors against esophageal cancer. J Enzyme Inhibit Med Chem. 2022;37(1):1995-2003. DOI: 10.1080/14756366.2022.2098954.
63. Yang Z, Yu GL, Zhu X, Peng TH, Lv YC. Critical roles of FTO-mediated mRNA m6a demethylation in regulating adipogenesis and lipid metabolism: Implications in lipid metabolic disorders. Genes Dis. 2022;9(1):51-61. DOI: 10.1016/j.gendis.2021.01.005.
64. Zhang B, Jiang H, Wu J, Cai Y, Dong Z, Zhao Y, *et al*. M6a demethylase FTO attenuates cardiac dysfunction by regulating glucose uptake and glycolysis in mice with pressure overload-induced heart failure. Signal Transduct Target Ther. 2021;6(1):377,1-3. DOI: 10.1038/s41392-021-00699-w.
65. Ben-Haim MS, Moshitch-Moshkovitz S, Rechavi G. FTO: linking m6a demethylation to adipogenesis. Cell Res. 2015;25(1):3-4. DOI: 10.1038/cr.2014.162.
66. Zhang Q, Riddle RC, Yang Q, Rosen CR, Guttridge DC, Dirckx N, *et al*. The RNA demethylase FTO is required for maintenance of bone mass and functions to protect osteoblasts from genotoxic damage. Proc Nat Acad Sci. 2019;116(36):17980-17989. DOI: 10.1073/pnas.1905489116.
67. Wu Y, Li J, Li C, Lu S, Wei X, Li Y, *et al*. Fat mass and obesity-associated factor (FTO)-mediated n6-methyladenosine regulates spermatogenesis in an age-dependent manner. J Biol Chem. 2023;299(6):104783,1-12. DOI: 10.1016/j.jbc.2023.104783.
68. Qiu W, Zhou Y, Wu H, Lv X, Yang L, Ren Z, *et al*. RNA demethylase FTO mediated RNA m6A modification is involved in maintaining maternal-fetal interface in spontaneous abortion. Front Cell Dev Biol. 2021;9:617172,1-13. DOI: 10.3389/fcell.2021.617172.
69. Tenn MW, Steacy LM, Ng CC, Ellis AK. Onset of action for loratadine tablets for the symptomatic control of seasonal allergic rhinitis in adults challenged with ragweed pollen in the environmental exposure unit: a post hoc analysis of total symptom score. Allergy Asthma Clin Immunol. 2018;14:5,1-7. DOI: 10.1186/s13223-017-0227-4.
70. Barenholtz HA, McLeod DC. Loratadine: a nonsedating antihistamine with once-daily dosing. DICP. 1989;23(6):445-450. DOI: 10.1177/106002808902300601.
71. Xie GY, Wu XN, Ling YY, Rui YL, Wu DY, Zhou JW, *et al*. A novel inhibitor of n-6-methyladenosine demethylase fto induces mRNA methylation and shows anti-cancer activities. Acta Pharm Sin B. 2022;12(2):853-866. DOI: 10.1016/j.apsb.2021.08.028.
72. Zheng GQ, Cox T, Tribbey L, Wang GZ, Iacoban P, Booher ME, *et al*. Synthesis of a FTO inhibitor with

anticonvulsant activity. Acs Chem Neurosci. 2014;5(8):658-665.
DOI: 10.1021/cn500042t.
73. Su R, Dong L, Li YC, Han L, Gao M, Wunderlich M, *et al*. Effective novel FTO inhibitors show potent anti-cancer efficacy and suppress drug resistance. Blood. 2019;134(1):1-5.
DOI: 10.1182/blood-2019-124535.
74. Chen B, Ye F, Yu L, Jia G, Huang X, Zhang X, *et al*. Development of cell-active n6-methyladenosine RNA demethylase FTO inhibitor. J Am Chem Soc. 2012;134(43):17963-17971.
DOI: 10.1021/ja3064149.
75. Huang Y, Yan J, Li Q, Li J, Gong S, Zhou H, *et al*. Meclofenamic acid selectively inhibits FTO demethylation of m6a over alkbh5. Nucleic Acids Res. 2015;43(1):373-84.
DOI: 10.1093/nar/gku1276.
76. Wang T, Hong T, Huang Y, Su H, Wu F, Chen Y, *et al*. Fluorescein derivatives as bifunctional molecules for the simultaneous inhibiting and labeling of FTO protein. J Am Chem Soc. 2015;137(43):13736-13739.
DOI: 10.1021/jacs.5b06690.
77. Peng S, Xiao W, Ju D, Sun B, Hou N, Liu Q, *et al*. Identification of entacapone as a chemical inhibitor of FTO mediating metabolic regulation through Foxo1. Sci TranslMed. 2019;11(488):eaau7116,1-12.
DOI: 10.1126/scitranslmed.aau7116.
78. Han X, Wang N, Li J, Wang Y, Wang R, Chang J. Identification of nafamostat mesilate as an inhibitor of the fat mass and obesity-associated protein (FTO) demethylase activity. Chem Biol Interact. 2019;297:80-84.
DOI: 10.1016/j.cbi.2018.10.023.
79. Huff S, Tiwari SK, Gonzalez GM, Wang Y, Rana TM. M(6)A-RNA demethylase FTO inhibitors impair self-renewal in glioblastoma stem cells. ACS Chem Biol. 2021;16(2):324-333.
DOI: 10.1021/acschembio.0c00841.